Effects of surface roughness and oxide layer on the thermal boundary conductance at aluminum/silicon interfaces

Patrick E. Hopkins,* Leslie M. Phinney, Justin R. Serrano, and Thomas E. Beechem
Sandia National Laboratories, Albuquerque, New Mexico 87185-0346, USA
(Received 7 June 2010; revised manuscript received 6 July 2010; published 5 August 2010)

In nanosystems, the primary scattering mechanisms occur at the interfaces between the material layers. As such, the structure and composition around these interfaces can affect scattering rates and, therefore, thermal resistances. In this work, we measure the room-temperature thermal boundary conductance of aluminum films grown on silicon substrates subjected to various pre-Al-deposition surface treatments with a pump-probe thermoreflectance technique. The Si surfaces are characterized with atomic force microscopy to determine mean surface roughness. The measured thermal boundary conductances decrease as Si surface roughness increases. In addition, stripping of the native oxide layer from the surface of the Si substrate immediately prior to Al film deposition causes the thermal boundary conductance to increase. The measured data are compared to an extension of the diffuse mismatch model that accounts for interfacial mixing and structure around the interface in order to better elucidate the thermal scattering processes affecting thermal boundary conductance at rough interfaces.

DOI: 10.1103/PhysRevB.82.085307 PACS number(s): 66.70.Df, 66.90.+r, 68.60.Dv

I. INTRODUCTION

Thermal boundary resistance between two solids[1] is a dominant thermal resistance in nanosystems.[2] The thermal boundary resistance, R, relates the temperature drop across an interface to the interfacial heat flux, Q, and is quantified as $R=\Delta T/Q$, where T is the temperature. The inverse of the thermal boundary resistance is the thermal boundary conductance, h. Typical values of h at solid-solid interfaces range from $\sim$500 to 10 MW m^{-2} K^{-1} ($R=2-100\times10^{-9}$ m^2 K W^{-1}) at room temperature depending on the solids adjacent to the boundary and the quality of the interfaces themselves.[2–4]

Nanomaterials with characteristic sizes less than carrier mean-free paths cause an increase in interfacial scattering events compared to the carrier scattering events in the "bulk" of the individual materials.[2] This increase in interfacial scattering causes the thermal resistance in nanosystems to be highly dependent on surface roughness, structure, interdiffusion, and reactions around the interface.[5–7] Several theoretical and numerical studies have investigated the effects of interfacial disorder and roughness on h (Refs. 8–15) but only recently has a relationship between h and interfacial properties been experimentally quantified.[6,7] Clearly, the lack of experimental work focusing on explicitly quantifying the relationship between the structural and thermal properties of an interface warrants further investigation into the variables affecting thermal boundary conductance.

In this paper, we study the thermal boundary conductance at Al/Si interfaces with varying substrate surface roughness. In addition, for a portion of the samples, we strip the native oxide layer and hydrogen terminate the Si surfaces to determine the thermal resistance associated with the native oxide layer. We measure the Al/Si thermal boundary conductances with time domain thermoreflectance. The resulting measurements imply that surface roughness and a native oxide layer decrease the thermal boundary conductance thereby verifying a distinct structure-property relationship for interfacial transport. The implications of this relationship, in turn, impact a range of applications including both boundary roughening efforts focused on increasing the figure of merit in thermoelectric nanomaterials[2,16–18] as well as the management of thermal transport at metalized semiconductor interfaces such as Schottky barriers and ohmic contacts.[19]

II. EXPERIMENTAL DETAILS

We prepare eight different Al/Si interfaces by evaporating 80 nm of pure Al (vacuum pressure $<10^{-7}$ Torr) on Si substrates subjected to different surface treatments prior to Al film deposition. The Si wafers were 500 μm thick, phosphorous doped (n type), and single crystalline (100) with an average resistivity of $\sim$1 Ω cm. All substrates were cleaned with methanol and acetone and rinsed in de-ionized water before Al evaporation. For sample 1, no further processing was performed prior to deposition (as received). Samples 2–4 were treated in buffered oxide etch (BOE) to remove the native SiO_2 layer on the surface of the wafer, submersed in tetramethyl ammonium hydroxide (TMAH) solution at 80 °C for various times, then left in ambient for over 24 h to allow the native oxide layer to reform on the surface. The TMAH treatment was used to increase the surface roughness of the Si surface. In a parallel batch of samples (samples 1a–4a), the same surface treatments were performed as samples 1–4 only the Si wafers were subjected to an additional BOE treatment immediately prior to loading into the evaporator in which the chamber was pumped down to low 10^{-7} Torr. These eight samples allowed us to independently study the effect of a roughened interface and the native SiO_2 layer on h. We list the surface treatment details for the samples in Table I.

We characterize the rms surface roughness, δ, of the samples prior to Al deposition with atomic force microscopy (AFM) at three random locations on the surface. As expected, the BOE treatment does not change the surface morphology of the Si, as the surface roughness of the Si of

TABLE I. Details of Si surface treatments prior to 80 nm Al film deposition, average roughness from the AFM scans, δ (nm), with standard deviation among the AFM scans, σ_δ, and average measured thermal boundary conductance h (MW m^{-2} K^{-1}) with standard deviation, σ_h. The reported standard deviations represent the deviation about the mean value of the multiple measurements on single sample.

Sample	Si treatment	δ	σ_δ	h	σ_h
1	As received	1.96	0.7	143.6	6.35
1a	BOE	1.4	0.5	193	17.7
2	BOE, 3 min 30 s TMAH at 80 °C, regrow native SiO_2	10.6	1.3	124.2	2.17
2a	BOE, 3 min 30 s TMAH at 80 °C, BOE	10.1	1.5	160.6	5.60
3	BOE, 5 min TMAH at 80 °C, regrow native SiO_2	8.56	1.0	133.4	9.42
3a	BOE, 5 min TMAH at 80 °C, BOE	6.62	1.1	158	7
4	BOE, 20 min TMAH at 80 °C,	6.71	2.7	114.6	2.3
4a	BOE, 20 min TMAH at 80 °C, BOE	5.56	2.4	170.4	3.36

samples with and without the BOE are very similar (e.g., samples 1 and 1a exhibit surface roughnesses of 1.96 nm and 1.4 nm, respectively). Figure 1 shows representative AFM surface profiles of the Si surface of samples 1 and 2. The differing surface roughnesses between the TMAH-treated and non-TMAH-treated samples are clearly discernible.

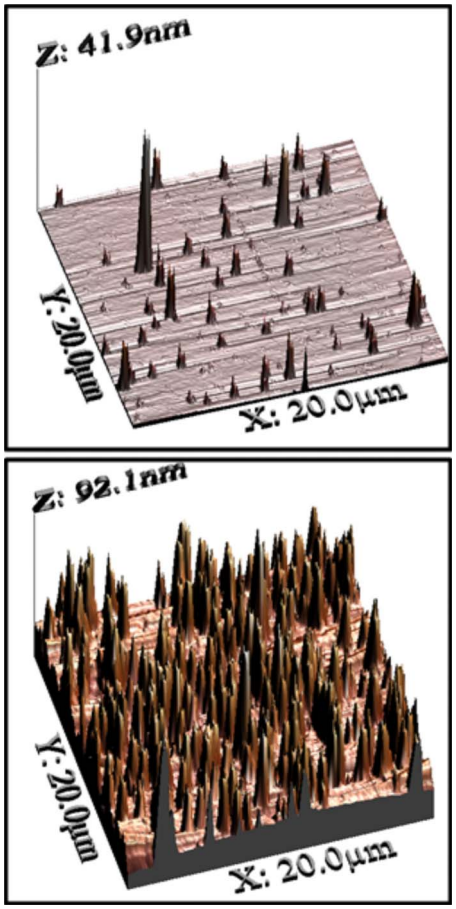

FIG. 1. (Color online) AFM three-dimensional surface profiles for samples 1a (top) and 2 (bottom), clearly demonstrating the differing surface roughness of the Si substrates prior to 80 nm Al film deposition

Since TMAH initiates Si removal around surface imperfections, the shorter TMAH treatments lead to rougher surfaces even though less volume of Si has been removed. Longer treatments result in smoother surfaces as the surface imperfections are etched away.

The time domain thermoreflectance (TDTR) experimental setup we use to measure h is nearly identical to similar setups that exploit coaxial pump-probe geometries discussed in previous works.[2,20,21] Specifics of our experimental setup and analysis considerations are discussed in a previous publication.[22] We modulate the pump pulses at a frequency of 11 MHz to ensure one dimensional, cross plane-dominated transport in the Al/Si samples.[21,22] This cross plane-dominated transport ensures that the interfacial structure we are most sensitive to is mean interfacial roughness, δ, and not any in-plane transport affected by the differing correlation lengths between surface structures. We took five scans at random locations on each of the samples; representative thermoreflectance signals from samples 1a and 2 are shown in Fig. 2. Note the signals analyzed in this study are the ratio of the real component of the lock-in signal to the imaginary component, $-X/Y$. The differing temporal decays are related

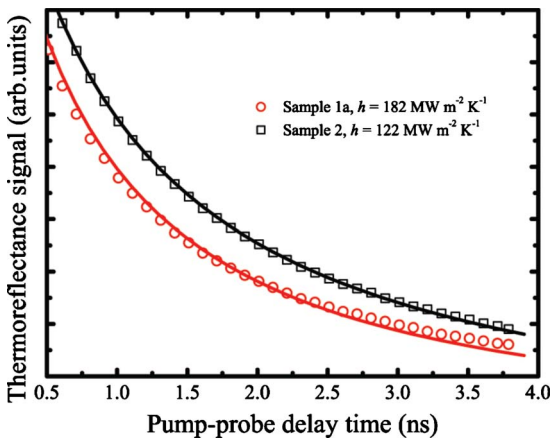

FIG. 2. (Color online) Two representative TDTR data on samples 1a and 2 along with the best-fit thermal model. The thermal boundary conductance, h, determined from the fits to theses specific data sets are listed.

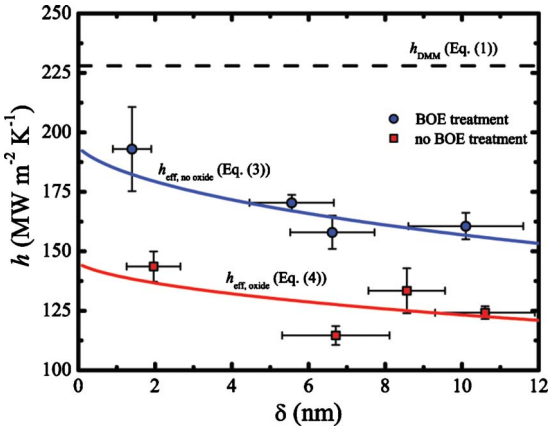

FIG. 3. (Color online) Predictions from Eq. (1) (DMM), Eq. (3) ($h_{\mathrm{eff,no\ oxide}}$), and Eq. (4) ($h_{\mathrm{eff,oxide}}$) as a function of interface roughness compared to the experimental data in Table I. The DMM has no functional dependency on interface roughness, whereas Eqs. (3) and (4) predict a decrease in h_{eff} with increasing roughness which is a trend observed in the experimental data.

to the change in thermal boundary conductances due to the different surface roughnesses. To quantify h in each of the samples, we fit the data with a two-layer (film/substrate) thermal model that accounts for pulse accumulation in the frequency domain.[23] Using h as the only free parameter, we use a least-squares fitting routine to determine h on each of the samples. Figure 2 shows the best-fit thermal models to the data and lists h for each of the data fits. The average h determined on each of the samples is listed in Table I along with the mean surface roughness. Standard deviations, σ, for both δ and h are also listed in Table I. For these fits, bulk material properties of Si are assumed and a bulk heat capacity of the 80 nm Al film is assumed.[24] We verify the film thicknesses with picosecond ultrasonics.[25,26] The thermal conductivity of the Al film was slightly reduced and estimated as 200 W m^{-1} K^{-1} from four-point probe electrical resistivity measurements, although in the time domain of our experiments slight changes in the Al film conductivity result in negligible changes to the best fit h. As apparent in Table I, not only does the surface roughness cause a change in h but removal of the native oxide layer also has an impact on h. The origins of these dependencies are analyzed in detail in the next section.

III. ANALYSIS

The measured thermal boundary conductances as a function of surface roughness for the series of Al/Si samples are plotted in Fig. 3 An increase in surface roughness leads to a decrease in h. In addition, the removal of the native SiO_2 layer leads to a fairly constant increase in h of more than 10%; from this we calculate the presence of the native oxide layer to add an average resistance of $1.74\times10^{-9}\pm9.0\times10^{-11}$ W^{-1} m^2 K. Taking the thermal conductivity of SiO_2 at room temperature, κ_{oxide}, as 1.24 W m^{-1} K^{-1} (Ref. 27), we estimate the native oxide layer thickness to be $d_{\mathrm{oxide}}=2.16\pm0.1$ nm.

To understand the carrier scattering processes contributing to thermal transport at the rough Al/Si interfaces, consider the thermal boundary conductance described by the diffuse mismatch model (DMM),[1] given by

$$h_{\mathrm{DMM}}=\frac{1}{4}\sum_j\int_{\omega_j}\hbar\omega D_{1,j}v_{1,j}\frac{\partial f}{\partial T}\alpha_{\mathrm{DMM},1\to2}d\omega, \qquad (1)$$

where side 1 refers to the Al and side 2 refers to the Si, $\hbar$ is the reduced Planck's constant, ω is the phonon angular frequency, D is the phonon density of states, v is the phonon group velocity, f is the phonon distribution, α is the phonon transmission probability, and the phonon flux integral is integrated into $j=3$ modes (one longitudinal and two transverse). From the principle of detailed balance on the incident phonon fluxes in the Al and Si, and assuming elastic phonon scattering,[28] the transmission coefficient is given by

$$\alpha_{\mathrm{DMM},1\to2}=\frac{\sum_j D_{2,j}v_{2,j}}{\sum_j D_{1,j}v_{1,j}+\sum_j D_{2,j}v_{2,j}}. \qquad (2)$$

To calculate the thermal boundary conductance using the DMM formulation, we assume a sine-type phonon dispersion[29,30] for the acoustic modes in Al and Si having a maximum longitudinal/transverse cutoff frequency as 60.4/36.5 Trad s^{-1} (Ref. 31) and 74.5/29 Trad s^{-1} (Ref. 32), respectively. The lattice parameters, meanwhile, are specified as 0.405 for the aluminum and 0.5430 nm within the silicon.[29] It is of note that the standard form of the DMM presented in Eqs. (1) and (2) assumes a perfect interface between the Al and Si (or any two materials for that matter). However, as demonstrated in this work, both the chemistry and structure around the interface can drastically affect the overall thermal boundary conductance. Consequently, the DMM over predicts the measured TBC as evidenced in Fig. 3.

In response to this fact, recent extensions to the DMM have accounted for structural disorder by considering a two-phase region around the interface.[8,33] These works have treated the two-phase region as either a single crystalline or fully disordered (amorphous) regime in the assessment of the phonon scattering. However, Al has been shown to form nanocrystallites in the transition layers around interface.[34] Therefore, to account for the observed reduction in thermal conductivity at the roughened interfaces, we consider a disordered nanocrystalline region of Al between the peaks and valleys on the silicon surface; i.e., the spatial extent of the nanocrystalline region is δ. Additionally, as the thermal boundary conductance at metal/semiconductor interfaces is dominated by phonon transport,[3] we do not consider electron effects.

The Al phonons will be subjected to multiple-scattering events in the disordered region for a spatial extent of δ before traversing across the Al/Si interface. In the samples in which the oxide layer was not removed prior to Al deposition (no BOE treatment), there will be an additional resistance from the native oxide layer. Therefore, the effective thermal boundary resistance is given by

$$h_{\text{eff,no oxide}} = \left(\frac{1}{h_{\text{DMM},1\to2}} + \frac{\delta}{\kappa_{\text{Al,int}}} \right)^{-1} \quad (3)$$

for the samples that were BOE treated and

$$h_{\text{eff,oxide}} = \left(\frac{1}{h_{\text{DMM},1\to2}} + \frac{\delta}{\kappa_{\text{Al,int}}} + \frac{d_{\text{oxide}}}{\kappa_{\text{oxide}}} \right)^{-1} \quad (4)$$

for the samples that were not BOE treated, where $\kappa_{\text{Al,int}}$ is the phonon thermal conductivity of the nanocrystalline Al region around the interface. We calculate the phonon thermal conductivity of this interfacial Al region with the Callaway-Holland-type model,[35,36] given by

$$\kappa_{\text{Al,int}} = \frac{1}{6\pi^2} \sum_j \int_q \hbar \omega D_j \frac{\partial f}{\partial T} v_j^2 \tau_{\text{Al,int},j} d\omega, \quad (5)$$

where $\tau_{\text{Al,int},j}$ is the overall phonon-scattering time of the Al phonons in this region. Scattering of the Al phonons will be dominated by the grain boundaries within the interfacial region and impurity scattering from elemental Si diffusion into the Al.[37] Umklapp scattering of Al phonons will negligibly contribute to the thermal resistance in this interfacial region since the three phonon mean-free path in Al is orders of magnitude larger than δ at room temperature.[38] Therefore, $\tau_{\text{Al,int},j} = (\tau_{\text{gb}}^{-1} + \tau_{\text{Si atoms}}^{-1})^{-1}$, where $\tau_{\text{gb}}^{-1} = v_j / \delta$ and $\tau_{\text{Si atoms}}^{-1} = A\omega^4$. The Al phonon-scattering rate with Si atoms takes the familiar form derived by Klemens.[39] In a more rigorous treatment of impurity scattering rates, the concentration and radii of the impurity atoms, the changes in the interatomic force constants, and the aharmonicities of the Al-Si bonds must be known to determine $\tau_{\text{Si atoms}}^{-1}$ (Ref. 40). As many of these parameters are difficult to determine around the two-phase interfacial region, we treat A as a fitting parameter which is constant for both Eqs. (3) and (4). This fit using A gives insight into the strength of impurity scattering around interfaces.

The resulting effective thermal boundary conductance for these interfaces using Eqs. (3) and (4) is shown in Fig. 3 with $A = 2.9 \times 10^{-43}$ s^3. Both models capture the trends and values in the experimental data with only a single fitting parameter between both models. The resulting values of A used to simultaneously fit Eqs. (3) and (4) is two orders of magnitude greater than that in naturally occurring Si (Si scattering with isotopes) but is similar in magnitude to the scattering strength observed in alloys.[41,42] This is consistent with our definition of the interfacial region around the rough Si surface as a two-phase alloy.

IV. CONCLUSIONS

In this paper, we study the thermal boundary conductance at Al/Si interfaces with different substrate surface roughness. In addition, we etch the native oxide layer and hydrogen terminates a portion of the Si interfaces to determine the thermal resistance associated with a native oxide layer. By measuring the Al/Si thermal boundary conductances with time domain thermoreflectance on these differently prepared substrates, surface roughness and a native oxide layer are shown to decrease the thermal boundary conductance. We investigate the functional dependency of the measured thermal boundary conductance with analytical models based on the diffuse mismatch model and show that in addition to phonon scattering at the Al/Si interface, phonon scattering in the Al due to Si mass impurities and boundaries in the nanocrystalline interfacial region contribute to the observed roughness dependency of the interfacial transport.

ACKNOWLEDGMENTS

P.E.H. is greatly appreciative for funding from the LDRD Program Office. The authors thank T. Harris at Sandia Laboratories for assistance with substrate surface preparation and D. Pete at Sandia Laboratories for assistance with characterization. This work was performed, in part, at the Center for Integrated Nanotechnologies, a U.S. Department of Energy, Office of Basic Energy Sciences user facility; the authors would like to thank John Sullivan for assistance regarding work at the Center for Integrated Nanotechnologies. Sandia National Laboratories is a multiprogram laboratory operated by Sandia Corporation, a wholly owned subsidiary of Lockheed Martin Corporation, for the United States Department of Energy's, National Nuclear Security Administration under Contract No. DE-AC04-94AL85000.

*pehopki@sandia.gov

[1] E. T. Swartz and R. O. Pohl, Rev. Mod. Phys. **61**, 605 (1989).
[2] D. G. Cahill, W. K. Ford, K. E. Goodson, G. D. Mahan, A. Majumdar, H. J. Maris, R. Merlin, and S. R. Phillpot, J. Appl. Phys. **93**, 793 (2003).
[3] H.-K. Lyeo and D. G. Cahill, Phys. Rev. B **73**, 144301 (2006).
[4] P. M. Norris and P. E. Hopkins, J. Heat Transfer **131**, 043207 (2009).
[5] E. T. Swartz and R. O. Pohl, Appl. Phys. Lett. **51**, 2200 (1987).
[6] P. E. Hopkins and P. M. Norris, Appl. Phys. Lett. **89**, 131909 (2006).
[7] P. E. Hopkins, P. M. Norris, R. J. Stevens, T. Beechem, and S. Graham, J. Heat Transfer **130**, 062402 (2008).
[8] T. E. Beechem, S. Graham, P. E. Hopkins, and P. M. Norris, Appl. Phys. Lett. **90**, 054104 (2007).
[9] D. Kechrakos, J. Phys.: Condens. Matter **2**, 2637 (1990).
[10] D. Kechrakos, J. Phys.: Condens. Matter **3**, 1443 (1991).
[11] A. G. Kozorezov, J. K. Wigmore, C. Erd, A. Peacock, and A. Poelaert, Phys. Rev. B **57**, 7411 (1998).
[12] R. S. Prasher and P. E. Phelan, J. Heat Transfer **123**, 105 (2001).
[13] S.-F. Ren, W. Cheng, and G. Chen, J. Appl. Phys. **100**, 103505 (2006).
[14] R. J. Stevens, L. V. Zhigilei, and P. M. Norris, Int. J. Heat Mass Transfer **50**, 3977 (2007).
[15] J.-Y. Duquesne, Phys. Rev. B **79**, 153304 (2009).
[16] M. S. Dresselhaus, G. Dresselhaus, X. Sun, Z. Zhang, S. B.

Cronin, T. Koga, J. Y. Ying, and G. Chen, Microscale Thermophys. Eng. **3**, 89 (1999).
[17] B. Poudel, Q. Hao, Y. Ma, L. Yucheng, A. Minnich, B. Yu, X. Yan, D. Wang, A. Muto, D. Vashaee, X. Chen, J. Liu, M. S. Dresselhaus, G. Chen, and Z. Ren, Science **320**, 634 (2008).
[18] S. Riffat and X. Ma, Appl. Therm. Eng. **23**, 913 (2003).
[19] S. M. Sze, *Physics of Semiconductor Devices*, 2nd ed. (Wiley, New York, 1981).
[20] D. G. Cahill, K. E. Goodson, and A. Majumdar, J. Heat Transfer **124**, 223 (2002).
[21] A. J. Schmidt, X. Chen, and G. Chen, Rev. Sci. Instrum. **79**, 114902 (2008).
[22] P. E. Hopkins, J. R. Serrano, L. M. Phinney, S. P. Kearney, T. W. Grasser, and C. T. Harris, J. Heat Transfer **132**, 081302 (2010).
[23] D. G. Cahill, Rev. Sci. Instrum. **75**, 5119 (2004).
[24] F. Incropera and D. P. DeWitt, *Fundamentals of Heat and Mass Transfer* (Wiley, New York, 1996).
[25] C. Thomsen, H. T. Grahn, H. J. Maris, and J. Tauc, Phys. Rev. B **34**, 4129 (1986).
[26] C. Thomsen, J. Strait, Z. Vardeny, H. J. Maris, J. Tauc, and J. J. Hauser, Phys. Rev. Lett. **53**, 989 (1984).
[27] D. G. Cahill and R. O. Pohl, Phys. Rev. B **35**, 4067 (1987).
[28] P. E. Hopkins and P. M. Norris, J. Heat Transfer **131**, 022402 (2009).
[29] C. Kittel, *Introduction to Solid State Physics* (Wiley, New York, 1996).
[30] G. Chen, J. Heat Transfer **119**, 220 (1997).
[31] G. Gilat and R. M. Nicklow, Phys. Rev. **143**, 487 (1966).
[32] W. Weber, Phys. Rev. B **15**, 4789 (1977).
[33] T. Beechem and P. E. Hopkins, J. Appl. Phys. **106**, 124301 (2009).
[34] M. N. Touzelbaev and K. E. Goodson, J. Thermophys. Heat Transfer **11**, 506 (1997).
[35] J. Callaway, Phys. Rev. **113**, 1046 (1959).
[36] M. G. Holland, Phys. Rev. **132**, 2461 (1963).
[37] J. O. McCaldin and T. C. McGill, in *Thin Films: Interdiffusion and Reactions*, edited by J. M. Poate, K. N. Tu, and J. W. Mayer (Wiley, New York, 1978) , p. 69.
[38] A. Mrzyglod and O. Weis, J. Low Temp. Phys. **97**, 275 (1994).
[39] P. G. Klemens, Proc. Phys. Soc., London, Sect. A **68**, 1113 (1955).
[40] G. P. Srivastava, *The Physics of Phonons* (Taylor & Francis, New York, 1990).
[41] D. G. Cahill, F. Watanabe, A. Rockett, and C. B. Vining, Phys. Rev. B **71**, 235202 (2005).
[42] D. G. Cahill and F. Watanabe, Phys. Rev. B **70**, 235322 (2004).